applied sciences

MDPI

Article

Potential Flood Risk Scenario and Its Effects on Landscape Composition Using Hydraulic Modeling (HEC-RAS) in Boğaçay Sub-Basin/Türkiye

Serdar Selim [1], Emine Kahraman [2], Ceren Selim [3], Rifat Olgun [2,*], Nihat Karakuş [2], Erhan Önen [4], Mesut Çoşlu [5], Zeynep R. Ardahanlıoğlu [6], Mert Çakır [7] and İsmail Çinar [6]

1 Department of Space Sciences and Technologies, Faculty of Science, Akdeniz University, 07070 Antalya, Türkiye; serdarselim@akdeniz.edu.tr
2 Vocational School of Serik G-S. Sural, Akdeniz University, 07500 Antalya, Türkiye; eminekahraman@akdeniz.edu.tr (E.K.); nkarakus@akdeniz.edu.tr (N.K.)
3 Department of Landscape Architecture, Faculty of Architecture, Akdeniz University, 07070 Antalya, Türkiye; cerenselim@akdeniz.edu.tr
4 Department of Agricultural Services, Izmir Metropolitan Municipality, 35250 İzmir, Türkiye; erhan.onen@gmail.com
5 Department of Landscape Architecture, Faculty of Engineering and Architecture, Mehmet Akif Ersoy University, 15200 Burdur, Türkiye; mesutcoslu@gmail.com
6 Vocational School of Fethiye Ali Sıtkı Mefharet Kocman, Mugla Sitki Kocman University, 48300 Muğla, Türkiye; zeyneprb@mu.edu.tr (Z.R.A.); icinar@mu.edu.tr (İ.Ç.)
7 Department of Landscape Architecture, Faculty of Architecture, Süleyman Demirel University, 32200 Isparta, Türkiye; mertcakir@sdu.edu.tr
* Correspondence: rifatolgun@akdeniz.edu.tr

Abstract: Flooding, one of the most destructive and recurrent natural catastrophes, causes severe loss of life and property. The destructive effect of floods has increased with climate change and unplanned urbanization. To prevent this devastation and find solutions to potential flooding, it is important to improve engineering, ecological, hydrological, and hydrogeological precautions, as well as potential flood simulations. Using hydraulic models to perform flood simulations is a common and successful approach globally. In this study, HEC-RAS (1D) was used to simulate three different flood scenarios on the Boğaçay sub-basin in Antalya, the most important tourism destination of Türkiye. Flood scenarios were developed based on the data of the floods that occurred in the region in 2003 and 2006, with measured flow rates of 1899.9 m^3/s and 1450 m^3/s, respectively, and with the maximum flow rate (2408 m^3/s) determined by the relevant ministry. Then, the landscape composition of the region at the sub-basin scale was determined and the impacts of flood scenarios on the landscape composition around the riverbed were evaluated. The results of the analysis show that the water height will increase, ranging from 1.4 m to 3.6 m, and the landscape composition of the region will be significantly affected by this increase in water height in the three different flood scenarios. Especially in the part where the river meets the sea, 580.74 ha of urban settlement is estimated to be damaged by flooding, according to the worst-case scenario. Finally, the study will guide decision-makers to take the necessary measures under the relevant scenarios.

Keywords: flood risk; HEC-RAS; landscape composition; flood scenario; Boğaçay sub-basin

check for updates

Academic Editor: Nathan J. Moore

Received: 7 November 2024
Revised: 19 December 2024
Accepted: 26 December 2024
Published: 30 December 2024

Citation: Selim, S.; Kahraman, E.; Selim, C.; Olgun, R.; Karakuş, N.; Önen, E.; Çoşlu, M.; Ardahanlıoğlu, Z.R.; Çakır, M.; Çinar, İ. Potential Flood Risk Scenario and Its Effects on Landscape Composition Using Hydraulic Modeling (HEC-RAS) in Boğaçay Sub-Basin/Türkiye. *Appl. Sci.* **2025**, *15*, 219. https://doi.org/10.3390/app15010219

Copyright: © 2024 by the authors. Licensee MDPI, Basel, Switzerland. This article is an open access article distributed under the terms and conditions of the Creative Commons Attribution (CC BY) license (https://creativecommons.org/licenses/by/4.0/).

1. Introduction

Climate change is causing severe impacts on hydrology at both global and regional scales, and developing countries often face the most catastrophic impacts [1]. As a result of

anthropogenic-induced climate change, the probability of large-scale climate catastrophes increases worldwide, and this causes severe loss of both life and property [2]. Moreover, the increasing urban population has caused the impacts of natural disasters to become more intense [3] and the threat of extreme climate changes to become more apparent [4]. Furthermore, due to climatic changes, even arid and semi-arid regions are exposed to unpredictable rainfall intensities and flash floods [5,6], the floods occurring because of sudden and heavy rainfall causing severe social, economic, and cultural damages [7–10]. This natural catastrophe, which causes loss of life and property, as well as disruption of natural ecosystems, also leads to changes in the land cover and landscape structure around the river basin.

Landscape structure involves the study of the composition and configuration of ecosystems at the landscape level [11]. While configuration refers to the fragmentation of habitats reflected at the landscape, class, and patch level for certain land use/land cover (LULC) types, composition mostly deals with land cover types that are exhibited at the courser scale, but both are caused by habitat conversion and loss [12]. In landscape ecology, landscape composition describes how many different patch types are present and how abundant they are in relation to one another. Examples of the composition of the landscape are the amount of forest or swamp, the length of the forest edge or the density of highways [13]. The impact of human activity on the Earth has grown significantly in recent decades, changing the topography, land cover, and cause of the composition and configuration changes [14,15]. Critical ecological effects, including desertification, soil erosion, changes in vegetation and land usage, etc., are linked to the change. Although there is typically a clear human source for the alteration, its shape and extent are also influenced by morphological factors such as elevation, geologic formation, orientation, and slope [16,17]. Considering these factors, it can be said that floods and overflows also change the landscape structure at the composition and configuration levels [18]. Therefore, floods are natural catastrophes that can change the land cover and landscape composition in the region where they occur in the short, medium, or long term and in this context have a negative impact on hydrological processes and the provision of ecosystem services [19,20].

Floods are usually caused by rapid runoff of high-intensity rainfall in a short period of time [21,22]. Floods are difficult to intervene in, since the water level peaks rapidly, and interventions and assessments are often made based on their impacts [23]. Nowadays, it is recognized that flood hazards are among the most frequent disasters due to climate change and environmental factors and that most flood events are recurrent [23]. For this reason, governments and communities are making great efforts to manage this critical challenge. Hydrological models are developed to simulate floods that could occur in the area by considering available recorded data from the past and predicted future climatic conditions to improve planning in flood-prone areas and manage these risks [24]. Hydraulic modeling tools can predict the spatial and temporal evolution of river behavior during a flood and the resulting inundation extent [25–27]. There are several approaches to model river flooding [28,29], ranging from simple one-dimensional models that require fewer data [30] to more detailed two- and three-dimensional models [31–33]. These approaches provide rapid and highly accurate flood forecasts using hydrological models that simulate flow depth and velocity with the use of various mathematical equations [34–36]. The most widely used software for flood risk modeling are HEC-RAS, FLO-2D, SRH-2D, IBER, MIKE SHE, TUFLOW, River-Flow2D, and LISFLOOD-FP [37,38].

The HEC-RAS 6.5 software developed by the U.S. Army Corps of Engineers (USACE) in Washington, DC, USA is capable of performing one-dimensional steady flow and one- and two-dimensional unsteady flow calculations, sediment transport/mobile bed calculations, modeling of past floods, determination of flood-prone areas, and generation of

different hydrological development scenarios [38–41]. The software is used in various studies due to its features such as data entry/editing, hydraulic analysis (river analysis, flood/inundation analysis, etc.), data storage and management, reporting, and graphical presentation of analysis results [42]. In this study, the HEC-RAS 6.5 software, which is a free open-source software that is most frequently used in flood risk mapping studies [37,43–47], was used.

HEC-RAS 6.5 software was chosen not only because of its widespread use in flood risk modeling but also because of its functional features and efficiency in terms of data processing [48]. The 1D modeling of the software is frequently used in studies because it offers user-friendly features for researchers, does not require expertise, produces fast results, and works with minimum input data [49]. This model, which is one-dimensional and assumes constant velocity and water level along the cross-section, gives remarkable results for the flow in the channel [50,51]. Although HEC-RAS 1D can accurately calculate channel processes, 2D is a superior choice for the evaluation of flood wave dynamics in the floodplain, when the capacity of the channel is exceeded and the flow is spread over a wide area [52–54]. However, the HEC-RAS 1D model has some limitations. One-dimensional modeling has less detail compared to 2D and may not represent flood dynamics and relief at a high level [44]. While 1D modeling is sufficient for modeling the main river system, 2D modeling is more advantageous in areas requiring higher hydrodynamic accuracy, and combined 1D/2D modeling is more advantageous in larger river systems [54]. Moreover, if the flow path of the water is not known completely or the flow path is changing, 2D modeling gives more accurate results. Although HEC-RAS 2D and combined 1D/2D have been revealed to perform better than 1D when using high spatial resolution topographic data [54], the availability of high spatial resolution satellite data (LIDAR, DEM, etc.) is limited in developing countries such as Türkiye due to its high cost. Taking all these into account, although HEC-RAS 2D and combined HEC-RAS 1D/2D models have performed better in modeling flood processes and flooding than HEC-RAS 1D, HEC-RAS 1D can be used efficiently in terms of computation-time-cost, especially in developing countries where severe floods have the potential to cause devastating damages [48]. Therefore, more case studies around the world are still needed to use and evaluate the HEC-RAS 1D model [52].

The study was carried out in the Boğaçay sub-basin, which flows into the Mediterranean Sea in Antalya, one of the most important tourism centers of Türkiye. The Boğaçay River meets the sea with the confluence of two main streams in the city by affecting/being affected by various ecosystems along its route. The fact that there are many recorded flood catastrophes in the area, especially the catastrophic impacts of the floods in 2003 and 2006, and the high probability of recurrence have been important factors in determining this area as a study area. The study aims to create flood simulations in the Boğaçay sub-basin and evaluate the possible impacts of these flood simulations on landscape composition. Initially, the natural threshold boundaries of the Boğaçay sub-basin were determined using a geographic information system (GIS). Then, due to the high probability of recurrence of severe floods occurring in the Boğaçay River, flood simulations were created using the flow values of the floods recorded in the sub-basin and the peak flow value determined by the General Directorate of State Hydraulic Works (DSI) [55]. The flood that occurred in the study area on 23 December 2003 as a result of sudden and heavy rains lasted for 3 days and 5 people lost their lives. Moreover, 27 village settlements and 6600 rural and urban areas in the region were seriously damaged and USD 1 million of economic damage was determined. Although the frequency of recurrence of this flood was determined as 194 years in the studies, a similar flood catastrophe similarly recurred on 17 October 2006 after 3 days of heavy rainfall. In the flood with a frequency of 32 years, approximately 2 km of the main highway was inundated, and many vehicles were flooded and damaged. In

this flood, the ground floors of the buildings in the urban area were severely damaged, but there were no deaths [56]. Moreover, floods occurred in this region as a result of sudden rainfall in 1994, 2018, and 2021, which were smaller in scale and caused no loss of lives but did cause environmental damage. These floods, which severely affected the ecosystems in the region, as well as human health and property damage, were the main factors in the selection of this region as the study area. Lastly, the impacts of potential flooding on the landscape composition in the study area were assessed.

2. Study Area

The Boğaçay sub-basin, which was determined as the study area, is located at the coordinates 36°52′1.02″ N and 30°37′4.65″ E within the borders of Konyaaltı/Antalya, one of the most important tourism destinations in Türkiye (Figure 1). The Boğaçay River in the study area, about 70 km long, originates in the Taurus Mountains and runs into the Mediterranean Sea west of Antalya city center. There is a variety of land cover and land use along its route, such as forest, agriculture, settlement, and natural vegetation, and it has a wealth of biodiversity in its surroundings [57]. According to the Köppen–Geiger climate classification, the study area is in the CSA group, with hot and dry summers and mild and rainy winters. The average annual temperature of the region is 17.4 °C and the average annual precipitation is 1215 mm [58].

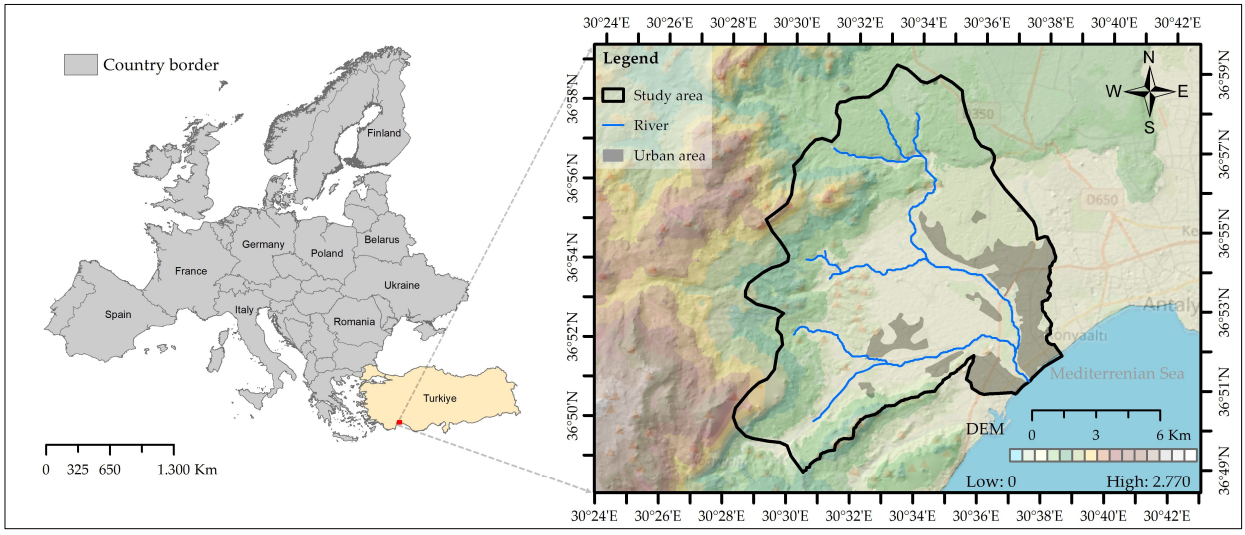


Figure 1. Location of the study area.

In Boğaçay, which has no regular flow, water accumulates mostly during rainy periods, and floods frequently occur during heavy rains (Figure 2). Although the amount of water in the riverbed decreases in summer due to evaporation, infiltration, and irrigation, floods occur in Boğaçay, which is fed by snow and precipitation waters in autumn and winter, especially after heavy rainfall in the winter season [59]. According to Turkish State Meteorological Service data, the average annual number of rainy days in the region is 73.5 days and the average annual rainfall is 1053.4 mm. The maximum daily rainfall recorded was 331.5 mm in 1969 [60]. While the main bed of the river is surrounded by agricultural areas and forests in the higher parts of the basin, most of the lower part of the river reaching the sea is surrounded by urban settlements. In the last 20 years, there has been a significant increase in urban settlements, especially in the low-slope region in the lower part of the river, which is most affected by floods. There are six bridges across the Boğaçay, two at the river mouth, two on the left river tributary (Çandır brook), and two on the right river tributary (Karaman brook). During the floods that occurred in the

region in the past years, particularly the two bridges at the river mouth were flooded and the bridges were closed to traffic for a while. At the river mouth of Boğaçay, 750 m long and 3 m high concrete barriers were built on both sides of the riverbed in 2018 for flood control purposes. However, the height of the water during the flood in 2021 exceeded these barriers; the bridges were closed to traffic and serious property losses occurred.



Figure 2. Key places in Boğaçay sub-basin. (**A**). The riverbed in Karaman brook and the agricultural and residential areas of the Aşağıkaraman neighborhood on its periphery. (**B**). The riverbed where the tributaries of the Çandır Brook converge and the agricultural and residential area in the Demircilik and Hacısekililer neighborhoods to the north of the river. (**C**). The riverbed of Karaman Brook near the city and the agricultural and residential areas of the Duraliler neighborhood. (**D**). Çandır Brook and the agricultural and residential areas in Demircilik and Hurma neighborhoods around the riverbed. (**E**). The region where the Boğaçay converges with the Mediterranean Sea and the surrounding settlements. Google Earth [61].

The study area has been affected by flood catastrophes in the past years due to sudden and intense rainfall, which caused severe destruction. Of the 179 flood disasters in Antalya province between 1975 and 2020, 57 occurred in the Konyaaltı district, which includes the Boğaçay River [62]. Moreover, there were major floods in the Boğaçay River in 2003 and 2006, resulting in serious environmental and economic damage in the region. In line with the data obtained from the past to the present, Boğaçay River has been reported as a river where floods occur frequently according to the frequency of flood occurrence on a river basis. The flood flow (Q_{100}) value of the Boğaçay River with a probability of recurrence in 100 years was calculated as 1355 m^3/s, the flood flow (Q_{500}) value with a probability of recurrence in 500 years was calculated as 1892 m^3/s, and the flood peak flow with a probability of recurrence in 500 years was calculated as 2408 m^3/s. In the flood that occurred in Boğaçay on 23 December 2003 as a result of heavy rainfall, which continued for 3 days, the flow rate was measured as 1988.9 m^3/s, and a 194-year recurrence was calculated. Likewise, in the flood that occurred in Boğaçay on 17 October 2006 as a result

of heavy rainfall, the flow rate was measured as 1450 m^3/s and a 31-year recurrence was calculated [56].

3. Methodology

The study consists of four stages: determining the sub-basin boundary, creating flood simulations, determining the landscape composition, and evaluating the simulations and landscape composition together.

3.1. Determination of the Sub-Basin Boundary

Alos Palsar Digital Elevation Model (DEM) data, which are freely available and have a spatial resolution of 12.5 m, were used to determine the sub-basin boundary [63]. First, the WGS84 UTM Zone36N projection was projected to DEM data by ArcGIS Pro 3.2.0 software. Then, fill/flow, direction/flow, accumulation/basin, and watershed were applied to DEM data using spatial analysis tools, respectively. The sub-basin including the Boğaçay River and its tributaries were determined by subsetting. Lastly, the river and its tributaries were converted into vector format and prepared for use in the HEC-RAS 6.5 software.

3.2. Generation of Flood Models in HEC-RAS

HEC-RAS 6.5 software developed by the USACE, which is freely available, was used to create flood scenarios. HEC-RAS 6.5 is capable of performing flood mapping with water surface profile results. Moreover, using the HEC-RAS 6.5 geometry and calculated water surface profiles, the flood depth and floodplain boundary are created through the RAS Mapper [64].

The DEM data (raster format) and river data (vector format) of the sub-basin created in the previous step were imported into the software. Then, the connections of the river system (river, bank lines, and flow paths) and cross-sections were determined. Bank lines delineate the primary channel boundaries within a cross-sectional profile. Flow paths are used to calculate the distances between sections in the left and right floodplain [64]. Flow paths were created downstream along the center of mass of the flow in the left and right floodplain. Cross-sections were generated based on the spatial arrangement of cross-section lines and the attributes of other layers, including the river, bank lines, and terrain layers. The cross-sections were positioned perpendicular to the anticipated flow direction in both the channel and overbank areas. The study area shows regular flow during heavy rains due to its topographical structure and defined boundaries along the channel and the river mouth structure that provides discharge in a certain period of time, and floods occur when the water height exceeds the bed boundaries. In this context, the steady flow analysis method, which requires constant flow data, was preferred since constant flow rates are used in the projections. The flow regime is determined as subcritical. Boundary conditions are needed to determine the initial water surface at the ends of the river system (upstream and downstream). An initial water surface is required for the program to start calculations. In a subcritical flow regime, boundary conditions are only necessary at the downstream ends of the river system [42]. At the downstream ends of the river system, the boundary condition is defined as the critical depth. Thus, the critical depth for each profile was automatically calculated by the software and used as a boundary condition. Then, Manning's roughness coefficients, which represent the resistance to flow in streams and floodplains and are represented in HEC-RAS 6.5 as "n" value, were calculated. Since the directional spreading of the overland flow depends on terrain roughness as well as topographic conditions, the Manning roughness coefficients are the most important parameters outside of geometry that conditions flow spreading [65]. Therefore, the geometry of the river (topography and bathymetry), boundary conditions (roughness, flow regime, etc.), and Manning roughness

coefficients are the factors that determine the outcomes of the hydrological model [66]. Manning's n value of the basin was created using actual data. Since there are no gauging stations in the basin, these data were prepared by selecting the data from the technical bulletin prepared by DSI for Boğaçay as a result of land surveys (Table 1). To determine the Manning roughness coefficients of the rivers in Türkiye, a technical bulletin is prepared by the DSI [55] and the Manning coefficients of the rivers can be calculated by the Cowan [67] method (Equation (1)) [68].

$$n = (n_0 + n_1 + n_2 + n_3 + n_4)m \quad (1)$$

where n_0: type of material in the riverbed, n_1: degree of channel irregularity, n_2: change in channel radius, n_3: similar effects of barriers, n_4: vegetation cover, and m: represents the degree of channel curvature.

Table 1. Roughness table for calculating Manning roughness coefficients [55].

Channel Conditions			Values
The material contained in the channel	Soil	n_0	0.020
	Rock		0.025
	Sand		0.024
	Gravel		0.028
Degree of disorder	Smooth	n_1	0.000
	Insignificant		0.005
	Intermediate		0.010
	Intense		0.020
Changes in channel radius	Gradual	n_2	0.000
	Occasionally changing		0.005
	Frequently changing		0.010–0.015
Similar effects of obstacles	Negligible	n_3	0.000
	Insignificant		0.010–0.015
	Significant		0.020–0.030
	Intense		0.040–0.060
Vegetation	Low	n_4	0.005–0.010
	Intermediate		0.010–0.025
	High		0.025–0.050
	Very high		0.050–0.100
Degree of curvature	Insignificant	m	1.000
	Significant		1.150
	Intense		1.300

In the technical bulletin prepared by the specialized flood commission of the DSI [55], the roughness table has been updated as follows (Table 1).

A land survey was carried out in the study area to select the relevant values in the roughness table. Accordingly, n_0: 0.028 (gravel), n_1: 0.010 (intermediate), n_2: 0.015 (frequently changing), n_3: 0.010 (insignificant); n_4: 0.020 (intermediate), and m: 1.150 (significant). Depending on the values determined in the land survey, the Manning roughness coefficients value of Boğaçay was calculated as 0.095, according to Equation (1).

After determining the basic inputs of the HEC-RAS 6.5 system, the river flow value needs to be determined and included in the system in order to create a flood scenario. At this stage, the flow values of the floods that have occurred in the past and are potentially recurring in the region and the peak flow value calculated by the Ministry of Forestry and Water Affairs (MFWA) [56] were used. According to MFWA [56], the peak flow rate

of Boğaçay (Q_{500}) is 2408 m^3/s. The flow rate in the 2003 flood in the region is Q_{194}: 1988.9 m^3/s and the flood flow rate in 2006 is Q_{31}: 1450 m^3/s. Using these flow rates, three different flood scenarios were created.

3.3. Determination of Landscape Composition with Land Cover Classification

In this study, the freely available global LULC map produced by Impact Observatory and Esri was used [69]. Sentinel-2 satellites are very useful for LULC mapping due to their high spatial, spectral, and temporal resolutions. Advances in deep learning and scalable cloud-based computing provide the analytical capability needed to realize the value of global satellite imagery observations. The developed LULC map is based on deep learning segmentation with a new and very large dataset of Sentinel-2 pixels. This model is a 10 m resolution global LULC map that enables automatic LULC mapping from time series observations and achieves state-of-the-art accuracy [70].

After obtaining the LULC digital map of the region from the https://livingatlas.arcgis.com/landcoverexplorer (accessed on 15 September 2024) website, subset operations were applied according to the sub-basin boundaries using ArcGIS Pro 3.2.0 Then, the stage of determining the landscape composition, which can be defined as the integrity formed by the combination of natural and artificial elements, was started. Landscape composition refers to the diversity of patch types within a landscape, usually measured using the proportions of different land cover types [71]. In determining the landscape composition, natural elements (water resources, vegetation, bare land, etc.) interact with cultural elements (agricultural areas, settlements, etc.) to create integrity [72]. Therefore, six classes of land cover types (water surface, settlement patch, green patch, agricultural patch, bare land, and sand/gravel) belonging to natural and artificial elements were identified for the study area, and landscape composition was defined (Figure 3).

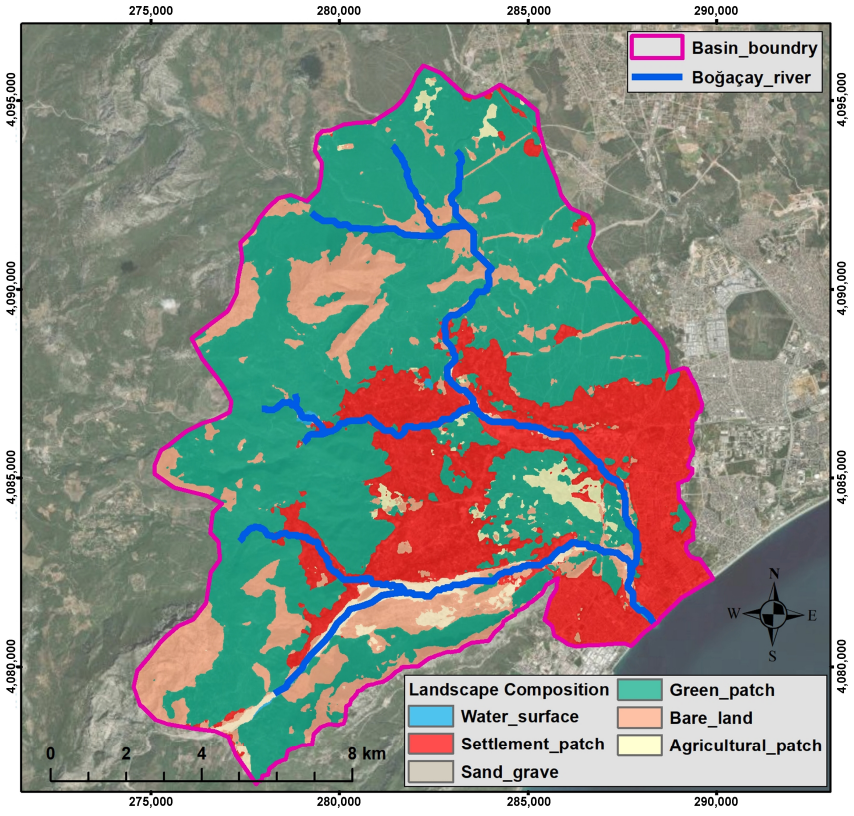


Figure 3. Landscape composition of Boğaçay sub-basin.

A natural lake with an area of approximately 35 ha is located on a tributary in the northwest of the sub-basin and is classified as a water surface. River and sea are excluded from the water surface class. The areas defined as green patches in the landscape composition are mostly forests and maquis. Also, urban green areas within the city are defined as green patches. The sand/gravel class, mostly bounding the riverbed, was formed by the deposition of sediments carried by floods in the past. The settlement patch is mostly made up of multi-story buildings, while bare land indicates barren terrain where no vegetation grows. Agricultural patches are areas around the riverbed where perennial crops (usually *Citrus sp.*) are grown.

3.4. Assessment of the Effects of Flood Scenarios on Landscape Composition

At the last stage of this study, the flood maps of three different flood scenarios were overlaid with the landscape composition map. In the overlay process, the proportional and spatial change in each class of landscape composition was determined. To determine the change, zonal statistics, which calculate the statistics of raster values in a different dataset, were used through ArcGIS Pro 3.2.0 software. Therefore, it was determined which land use was affected by the flood scenarios on the current landscape composition and to what extent. Then, the changes caused by different flood scenarios on the landscape composition were evaluated and interpreted on the basis of landscape ecology.

4. Results

4.1. Hydraulic Modeling Output for Different Flood Scenarios

Three different flood scenarios were created based on the flow rates of the two largest floods (2003–1988.9 m^3/s, 2006–1450 m^3/s) that occurred in the region in the past years and the peak flow rate (2408 m^3/s) determined by the relevant public institutions for the region (Figures 4–6).

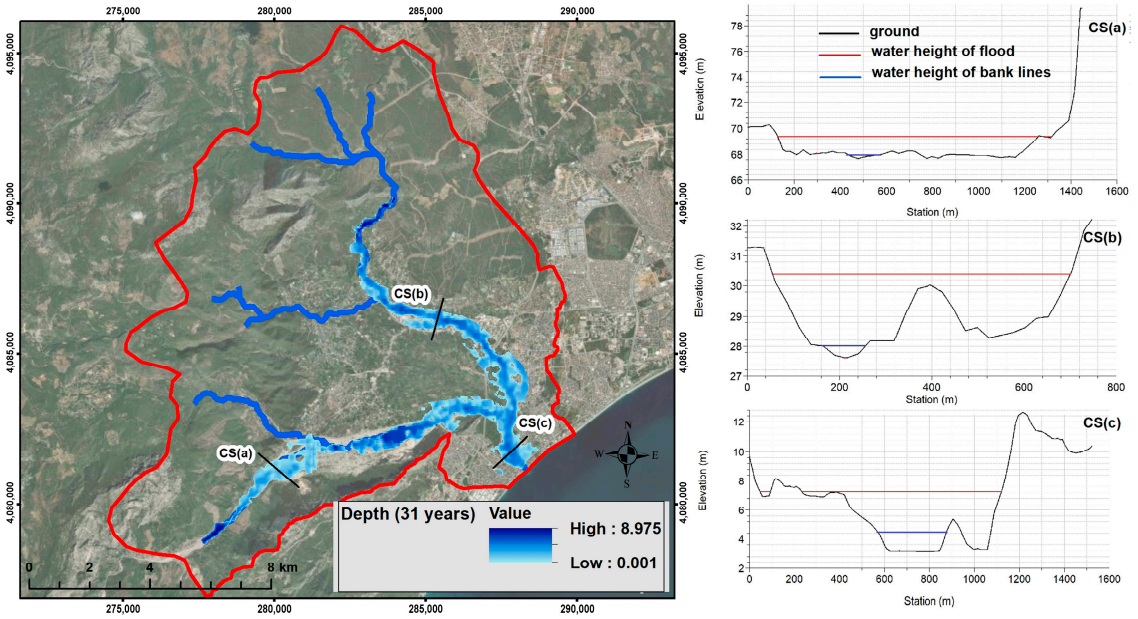


Figure 4. Thirty-one-year flood scenario.

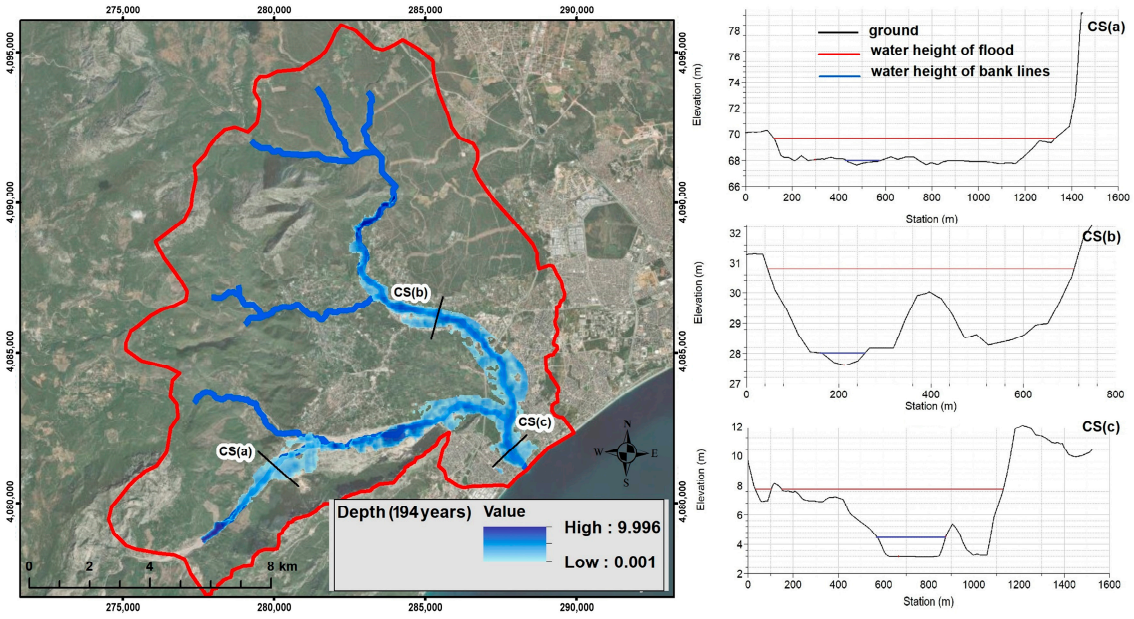


Figure 5. One-hundred-and-ninety-four-year flood scenario.

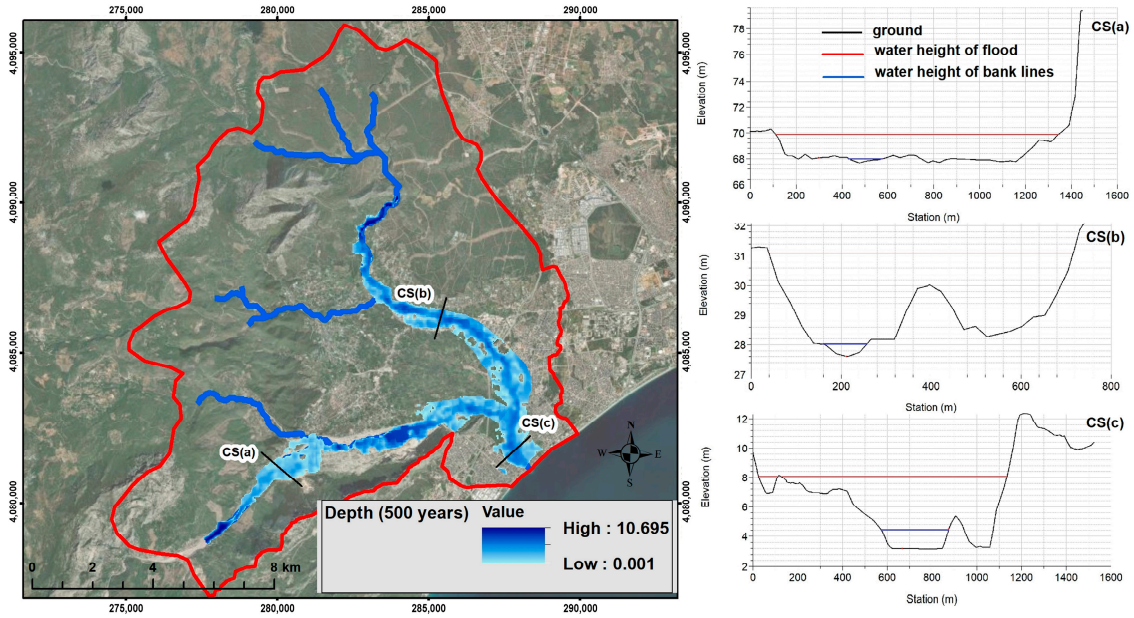


Figure 6. Five-hundred-year flood scenario.

The cross-sections were taken at three different important points of the river tributaries, and the current bank line height in the river and the water height in the potential flood were shown at these areas. Cross-section a ($CS_{(a)}$) is one of the main tributaries coming from the west of the river and affecting mostly agricultural lands. Cross-section b ($CS_{(b)}$) is one of the main tributaries coming from the north and is mostly surrounded by settlement patches. Cross-section c ($CS_{(c)}$) shows the cross-section formed by the confluence of two main tributaries, connected to the sea, located within the city center, and surrounded by an artificial bank line. Since $CS_{(c)}$ is in the most densely populated urban area, the possible water heights of the cross-section in this area according to the three flood scenarios are shown in Figure 7.

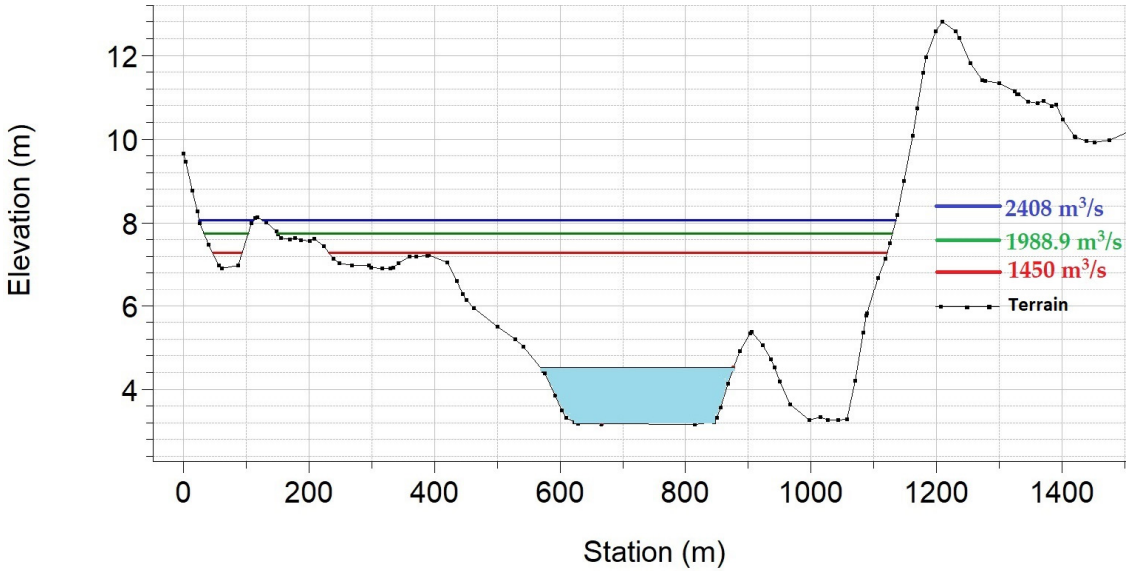


Figure 7. All values for $CS_{(c)}$.

In the flood simulation with a flow rate of 1450 m^3/s and a probability of recurrence in 31 years, the maximum depth is approximately 9 m. The land structure in the upper tributaries of the river is steep, and the deep valley formation indicates that flooding is unable to cause serious damage in these areas. However, the water flows out of the riverbed as it gets closer to the meeting point of the river with the sea, due to the partially flat terrain and shallow riverbed. According to the simulation, it is estimated that 1.4 m of water will rise in $CS_{(a)}$, 2.4 m in $CS_{(b)}$, and 2.8 m in $CS_{(c)}$.

In the flood simulation with a flow rate of 1988.9 m^3/s and a probability of recurrence in 194 years, the maximum depth is approximately 10 m. According to the simulation, $CS_{(a)}$ is predicted to rise by 1.7 m, $CS_{(b)}$ by 2.8 m, and $CS_{(c)}$ by 3.2 m. A water height increase of approximately 1 m is predicted compared to Q_{31}: 1450 m^3/s.

According to the flow rate calculated by MFWA [48], Q_{500}: 2408 m^3/s, the maximum depth in the flood simulation is approximately 10.7 m. It is predicted that the water will rise in $CS_{(a)}$ by 1.9 m, $CS_{(b)}$ by 3.1 m, and $CS_{(c)}$ by 3.6 m.

In the $CS_{(c)}$ section at the mouth of the river that connects from the city to the sea, the bank line border height is around 4.5 m. The active water surface height within the bank line varies depending on seasonal precipitation. If this maximum water height is exceeded by a potential flood, environmental land uses will be affected. In three different simulations in this section, it is seen that the water height can increase by 2.8 m in 31 years, 3.2 m in 194 years, and 3.6 m in 500 years.

4.2. Effects of Flood Scenarios on Landscape Composition

The landscape composition map of the sub-basin was generated from the Sentinel-2 Land Cover Explorer, a new web-based mapping application built on the ArcGIS Pro 3.2.0 API for JavaScript [69]. Using Sentinel-2 images with 10 m resolution and dated 2023, the landscape composition of the land was defined in six classes. According to the sub-basin boundaries, the region including the Boğaçay River and its tributaries is a total of 17,088.2 ha. It consists of a 67.8 ha water surface, a 9450.9 ha green patch, a 279.6 ha agricultural patch, a 4078 ha settlement patch, 410.9 ha of sand/gravel, and 2801 ha of bare land (Figure 8).

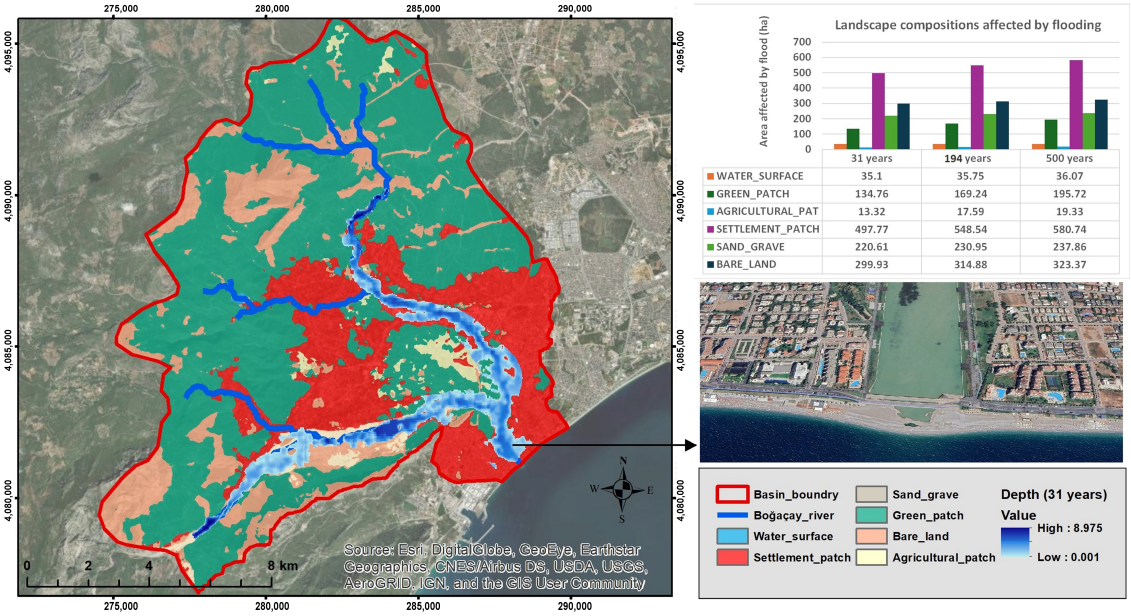


Figure 8. Interaction of floods and landscape composition.

According to the 31-year flood scenario, 35.1 ha (51.7%) of the water surface, 134.76 ha (0.1%) of the green patch, 13.32 ha (0.4%) of the agricultural patch, 497.7 ha (12.2%) of the settlement, 220.61 ha (53.6%) of the sand/gravel, and 299.93 ha (10%) of the bare land are affected by flooding. For the 194-year flood scenario, 35.75 ha of the water surface, 169.24 ha of the green patch, 17.59 ha of the agricultural patch, 548.54 ha of settlement, 230.95 ha of the sand/gravel, and 314.88 ha of the bare land are affected by flooding. Based on the 500-year flood scenario, 36.07 ha of the water surface, 195.72 ha of the green patch, 19.33 ha of the agricultural patch, 580.74 ha of the settlement, 237.86 ha of the sand/gravel, and 323.37 ha of the bare land are affected by flooding.

5. Discussion

Rivers are important components of the natural landscape and play a critical role in the health of ecosystems. However, as a result of climate change and human activities, river flooding significantly impacts both natural and artificial landscape composition. These floods have become a severe problem affecting urban public safety and a major factor limiting the economic and social development of the country. Due to rapid urbanization and changes in landscape composition, flood risk shows an increasing trend [73]. The study has revealed that potential flooding is a serious threat in the study area. The catastrophic effects of floods and floods that occurred in the basin in the past years, together with the changing land use since then, become more catastrophic in the current scenarios. Especially the coastal zone, where urban settlements are dense and the river discharges into the sea, is under serious flood threat. According to the 500-, 194-, and 31-year flood scenarios, 580.74 ha, 548.54 ha, and 497.7 ha of urban settlements in the study area are affected by flooding, respectively. According to the scenarios, although bare land and sand/gravel are the classes that will be most affected by floods, the classes that may face the worst social and economic consequences of potential flooding are urban settlements and agricultural areas. In the scenario created based on the maximum flow amount calculated by the relevant public institutions in Türkiye for the region, about 580 ha of settlements and about 20 ha of agricultural land are under flood risk. It is clearly seen that any flood in the study area, which is one of the most important tourism destinations of Türkiye and has a dense population, may cause tremendous loss of life and property. As a matter of fact, the devastation caused by floods in the region in the past years confirms this argument.

According to the MFWA [56] Antalya Basin Flood Management Plan, five people lost their lives, the drinking water and sewerage network was damaged, 6600 da areas were damaged, 27 villages and 1673 farms in rural areas were damaged in the flash flood that occurred in 2003 in Boğaçay. The economic loss of this flood catastrophe was estimated to be about USD 1 million. Moreover, during the rainfall-induced flash flood in 2006, a 1.7 km section of the Antalya-Alanya highway was flooded, many vehicles were dragged away, and hotels, workplaces, and residences located at low altitudes were damaged. Considering that the population of the region has more than doubled in the last 20 years and urbanization has expanded significantly, the magnitude of the potential risk is clearly seen.

The way to mitigate flood risk is to support the riverbed with suitable land management and structural practices. The flood scenarios in this study are based on the flow rates of the floods that occurred in the region in 2003 and 2006, which had catastrophic effects, and the maximum flow rates determined by the relevant public institutions for the region and the probability of recurrence. Therefore, short-, medium-, and long-term flood scenarios with specific intervals and considering climatic data have not been produced. Due to continuing changes in climate and the historical flood data covered by this study, it is difficult to assess the probability of flash flooding in the region. Floods are characterized by short periods of time and high flow velocities. Since the spatial distribution of flash floods is often determined by climatic conditions, land structure, topography, and LULC [9], consideration of these variables is crucial in preventing flood threat. The possibility of flash flooding can also be assessed by performing 2D and 3D hydrological modeling with a large number of variables [73]. Moreover, the use of high-resolution DEM and digital surface model (DSM) data in these hydrological models will enable more precise determination of flood impact areas.

The potential floods in the region have the potential to directly affect human settlements. Urbanization and gray infrastructure projects increase flood risk and change both the natural landscape and settlements. While gray infrastructure is often built to manage flooding, sometimes it obstructs natural flows, causing more problems [74]. Developing emergency intervention and prioritization policies against possible flood risk, especially in urban areas, is an important issue in minimizing the loss of life and property. As is known, the resilience of a city facing a flood disaster depends on the structural characteristics of buildings and the evacuation and intervention capacities. This situation could be interpreted as the past flood disasters in the Boğaçay sub-basin have reduced the resilience of the city. Therefore, analyzing changes in urban resilience using risk-based recovery under various scenarios will help to develop effective intervention strategies [3].

The floods may change the soil structure as the water level rises much higher than normal, raising groundwater levels. The materials (sediment) brought by floods can change the nutrient value of the soil and cause erosion and landslides [75]. Due to the topography of the basin and sudden changes in slope, a potential flood disaster can also bring the risk of landslides. River flooding also has drastic impacts on vegetation. High water levels can destroy the root systems of plants, which can destabilize local ecosystems. In particular, plant species living in waterlogged areas along the Boğaçay River are at risk of further damage following floods [76]. Floods also change the dynamics of ecosystems in the region. Flooding affects biodiversity in areas where aquatic and terrestrial habitats converge. In the long term, floods can cause the spread of aquatic species and the disappearance of some terrestrial species in the region [77].

The effects of flooding on landscape composition according to the scenarios in the study area are important issues to be considered in landscape design and planning. In areas at risk of flooding, sustainable design approaches should be adopted, natural processes should be supported, and human activities should be minimized.

Long-term flooding of agricultural lands can lead to loss of topsoil and moderate to severe erosion phase change, resulting in reduced crop yield potential [78]. One of the most widely cultivated and widely consumed fruit species worldwide, citrus fruits, are generally intolerant to flood stress [79]. Studies have shown that flooding of citrus species results in adverse effects such as decreases in root hydraulic conductivity [80] and root rot [81]. Türkiye has a significant share in world citrus production and ranks second in the world in citrus exports. In 2022, approximately 4.7 million tons of citrus fruits were produced in Türkiye, with most of this production concentrated in Antalya [82]. Especially the agricultural areas around Boğaçay are prominent in terms of citrus production. When three different flood scenarios are evaluated, it is predicted that agricultural lands in the region will be adversely affected by potential flooding, and this will lead to serious losses in the agricultural sector.

Planning blue-green infrastructure systems, a nature-based solution to flooding increases urban flood control while at the same time protecting biodiversity [83]. Landscape architects and urban planners should integrate water management strategies into plans when assessing the potential impacts of flooding. Urban plans prepared in this context will ensure the protection and restoration of natural drainage systems, management of watersheds, and protection of pre- and post-flood vegetation.

Floods are complex processes that affect the composition of natural and artificial landscapes, and understanding these processes is critical for sustainable landscape design and management. Regarding the impacts of future climate scenarios, flood management and landscape reshaping [84] are imperative to increase the resilience of human communities and ecosystems.

The region where the study area is located is still at risk of flooding due to sudden and heavy rainfall and mostly anthropogenic land use changes. In this study, the HEC-RAS 1D model was used to simulate the potential effects of flow rates from past flood catastrophes on the current riverbed. The advantage of this model is that it can produce fast and practical results at medium and small scales with less data and without requiring expertise. However, it is limited in providing high accuracy expectations in real-time flood phenomena. Nevertheless, 1D hydraulic modeling using data based on LiDAR-derived DEMs can produce sufficiently accurate information on flood hazards as stated by Huţanu et al. [48]. Among them is LISFLOOD-FP [85], an efficient hydrodynamic model for calculating potential flooding over complex topography, the two-dimensional rainfall-runoff and flood inundation (RRI) model that treats hill slopes and river channels separately [86], the 2D hydrodynamic (HM2D) model for simulating complex flow patterns [87], HEC-HMS, a physically based and conceptually semi-distributed model [88], the 1dCNN model developed as an alternative to high-resolution hydrodynamic models by Kabir et al. [89], the LSTM-SRR model by Zhou et al. [90], the GP-EOF model by Donnelly et al. [91], and the LSTM-EOF model by Hu et al. [92]; these are some of the current and improved flood models. Moreover, as stated by Aryal et al. [93] and Zainal and Talib [94], the HEC-RAS model is calibrated with the past data and confirmed with the current data. However, since there is no gauge station within the study area, it was not possible to verify Manning's n with current data. However, the calibration process was carried out using the data in the technical bulletin prepared for the Boğaçay River by DSİ, the official institution, through the data of the past periods. The installation of a gauge station in the study area will remove the limitation of obtaining up-to-date data (daily flows, peak flows, etc.) for future studies. This study provides a general framework for the potential flooding of the Boğaçay River, but it is recommended to use more advanced models as mentioned above to produce deeper and more accurate flood simulations of the basin.

6. Conclusions

In this study, three different flood scenarios were developed based on the flow rate of the floods that occurred in the region in the past years and the maximum flow rate calculated by the relevant official agencies for the region, and the impact of these potential floods on the landscape composition was evaluated. In this context, generating different scenarios by evaluating the existing flood data and potential flood probabilities together and evaluating the impact of possible floods on landscape composition constitute the original value of the study. According to the results obtained, it has been determined that potential floods in the Boğaçay sub-basin due to climate change and sudden alterations in precipitation will cause significant damage on the landscape composition. It is predicted that damages that may occur, especially in the settlement and agricultural patches within the landscape composition classes, will cause serious loss of life and property.

This flood risk assessment may constitute an important part of the implementation of risk management in the area. The results will provide a scientific basis for the implementation of various structural, vegetative, and sociological measures for flood prevention, mitigation, and prioritization. It may also contribute to raising awareness of flood risk prevention among local people and assist flood prevention and mitigation departments to take effective measures to cope with floods.

Overall, the Boğaçay sub-basin is at severe risk of flooding, and to prevent flooding, mitigate its impact, and develop strategies to intervene against potential flooding, it is necessary to first develop flood risk scenarios, as was done in this study, and then design and implement a series of geological, ecological, hydrological, and engineering measures accordingly. The potential flooding of the Boğaçay sub-basin in Konyaaltı can be put under control only in this way.

Author Contributions: Conceptualization, S.S., C.S., E.K., R.O. and N.K.; methodology, S.S., R.O., N.K. and E.Ö.; software, S.S., R.O. and N.K.; validation, C.S., E.Ö., Z.R.A., M.Ç. (Mesut Çoşlu) and M.Ç. (Mert Çakır); formal analysis, S.S., N.K., C.S. and M.Ç. (Mesut Çoşlu); investigation, C.S., R.O., E.K., E.Ö., Z.R.A. and M.Ç. (Mesut Çoşlu); resources, C.S., E.K., E.Ö., Z.R.A., M.Ç. (Mert Çakır) and İ.Ç.; data curation, S.S., C.S., N.K. and M.Ç. (Mert Çakır); writing—original draft preparation, S.S., R.O., N.K. and C.S.; writing—review and editing, S.S., C.S., E.K., R.O., N.K., E.Ö., M.Ç. (Mesut Çoşlu), Z.R.A., M.Ç. (Mert Çakır) and İ.Ç.; visualization, S.S. and N.K.; project administration, S.S. All authors have read and agreed to the published version of the manuscript.

Funding: This research received no external funding.

Institutional Review Board Statement: Not applicable.

Informed Consent Statement: Not applicable.

Data Availability Statement: The data presented in this study are available on request from the corresponding author due to their reuse in future studies planned to be conducted in the same region using different models.

Conflicts of Interest: The authors declare no conflicts of interest.

References

1. Toosi, A.S.; Doulabian, S.; Tousi, E.G.; Calbimonte, G.H.; Alaghmand, S. Large-scale flood hazard assessment under climate change: A case study. *Ecol. Eng.* **2020**, *147*, 105765. [CrossRef]
2. Natkaniec, W.; Godyń, I. Urban flood risk assessment and mapping using gis-dematel method: Case of the Serafa River Watershed, Poland. *Water* **2024**, *16*, 2636. [CrossRef]
3. Park, H.J.; Song, S.M.; Kim, D.H.; Lee, S.O. Socioeconomic impact on urban resilience against flood damage. *Appl. Sci.* **2024**, *14*, 7882. [CrossRef]
4. Sun, Q.; Nazari, R.; Karimi, M.; Rabbani Fahad, M.G.; Peters, R.W. Comprehensive flood risk assessment for wastewater treatment plants under extreme storm events: A case study for New York City, United States. *Appl. Sci.* **2021**, *11*, 6694. [CrossRef]

5. Bekele, D.; Alamirew, T.; Kebede, A.; Zeleke, G.; Melesse, A.M. Modeling climate change impact on the hydrology of Keleta watershed in the Awash River basin, Ethiopia. *Environ. Model Assess.* **2019**, *24*, 95–107. [CrossRef]
6. Meerow, S.; Helmrich, A.M.; Andrade, R.; Larson, K.L. How do heat and flood risk drive residential green infrastructure implementation in Phoenix, Arizona? *Urban Ecosyst.* **2021**, *24*, 989–1000. [CrossRef]
7. Watson, G.; Ahn, J.E. A systematic review: To increase transportation infrastructure resilience to flooding events. *Appl. Sci.* **2022**, *12*, 12331. [CrossRef]
8. Gacu, J.G.; Monjardin, C.E.F.; Senoro, D.B.; Tan, F.J. Flood risk assessment using gis-based analytical hierarchy process in the Municipality of Odiongan, Romblon, Philippines. *Appl. Sci.* **2022**, *12*, 9456. [CrossRef]
9. Gawrysiak, L.; Baran-Zgłobicka, B.; Zgłobicki, W. Flash Floods hazard to the settlement network versus land use planning (Lublin Upland, East Poland). *Appl. Sci.* **2024**, *14*, 8425. [CrossRef]
10. Baltaci, E.; Kalin, L.A. Low-impact development-based modeling framework for flood mitigation in a coastal community. *Water* **2024**, *16*, 2772. [CrossRef]
11. Mitchell, M.G.; Bennett, E.M.; Gonzalez, A. Linking landscape connectivity and ecosystem service provision: Current knowledge and research gaps. *Ecosystems* **2013**, *16*, 894–908. [CrossRef]
12. Echeverria, C.; Coomes, D.A.; Hall, M.; Newton, A.C. Spatially explicit models to analyze forest loss and fragmentation between 1976 and 2020 in southern Chile. *Ecol. Model.* **2008**, *212*, 439–449. [CrossRef]
13. Turner, M.G.; Gardner, R.H. *Quantitative Methods in Landscape Ecology*, 1st ed.; Springer-Verlag: New York, NY, USA, 1991; p. 458.
14. Tolessa, T.; Senbeta, F.; Kidane, M. Landscape composition and configuration in the central highlands of Ethiopia. *Nat. Ecol. Evol.* **2016**, *6*, 7409–7421. [CrossRef] [PubMed]
15. Aghakhani, M.; Nasrabadi, T.; Vafaeinejad, A. Assessment of the effects of land use scenarios on watershed surface runoff using hydrological modelling. *Appl. Ecol. Environ. Res.* **2018**, *16*, 2369–2389. [CrossRef]
16. Subedi, P.; Subedi, K.; Thapa, B. Application of a hybrid cellular automaton–markov (ca-markov) model in land-use change prediction: A case study of saddle creek drainage basin, Florida. *Appl. Ecol. Environ. Sci.* **2013**, *1*, 126–132. [CrossRef]
17. Yaghoobi, M.; Vafaeenejad, A.; Moradi, H.; Hashemi, H. Analysis of landscape composition and configuration based on LULC change modeling. *Sustainability* **2022**, *14*, 13070. [CrossRef]
18. Li, J.; Liu, X.; Wang, Y.; Li, Y.; Jiang, Y.; Fu, Y.; Wu, J. Landscape composition or configuration: Which contributes more to catchment hydrological flows and variations? *Landscape Ecol.* **2020**, *35*, 1531–1551. [CrossRef]
19. Xue, L.; Zhu, B.; Wu, Y.; Wei, G.; Liao, S.; Yang, C.; Wang, J.; Zhang, H.; Ren, L.; Han, Q. Dynamic projection of ecological risk in the Manas River basin based on terrain gradients. *Sci. Total Environ.* **2019**, *653*, 283–293. [CrossRef] [PubMed]
20. Yuan, Y.; Fang, G.; Yan, M.; Sui, C.; Ding, Z.; Lu, C. Flood-landscape ecological risk assessment under the background of urbanization. *Water* **2019**, *11*, 1418. [CrossRef]
21. Atif, R.M.; Siddiqui, M.H.; Almazroui, M. Near-real-time spatiotemporal analysis of convection and extreme rainfall leading to a flash flood using MSG-SEVIRI and TRMM data: A case study of a flash flood in Jeddah, Saudi Arabia on the November 25, 2009. *J. Flood Risk Manag.* **2020**, *13*, e12611. [CrossRef]
22. Sun, N.; Li, C.; Guo, B.; Sun, X.; Yao, Y.; Wang, Y. Urban flooding risk assessment based on FAHP-EWM combination weighting: A case study of Beijing. *Geomat. Nat. Hazards Risk* **2023**, *14*, 2240943. [CrossRef]
23. Bashir, B.; Alsalman, A. Flooding hazard vulnerability assessment using remote sensing data and geospatial techniques: A case study from Mekkah province, Saudi Arabia. *Water* **2024**, *16*, 2714. [CrossRef]
24. Toosi, A.S.; Calbimonte, G.H.; Nouri, H.; Alaghmand, S. River basin-scale flood hazard assessment using a modified multi-criteria decision analysis approach: A case study. *J. Hydrol.* **2019**, *574*, 660–671. [CrossRef]
25. Bulti, D.T.; Abebe, B.G. A review of flood modeling methods for urban pluvial flood application. *Model. Earth Syst. Environ.* **2020**, *6*, 1293–1302. [CrossRef]
26. Kumar, V.; Sharma, K.V.; Caloiero, T.; Mehta, D.J.; Singh, K. Comprehensive overview of flood modeling approaches: A review of recent advances. *Hydrology* **2023**, *10*, 141. [CrossRef]
27. Shin, J.; Rhee, D.S.; Park, I. Analysis of inundation flow characteristics and risk assessment in a subway model using flow simulations. *Appl. Sci.* **2024**, *14*, 8096. [CrossRef]
28. Sarchani, S.; Seiradakis, K.; Coulibaly, P.; Tsanis, I. Flood inundation mapping in an ungauged basin. *Water* **2020**, *12*, 1532. [CrossRef]
29. Louis, R.; Zech, Y.; Joseph, A.; Gonomy, N.; Soares-Frazao, S. Flood modeling of the June 2023 flooding of Léogâne city by the overflow of the Rouyonne River in Haiti. *Water* **2024**, *16*, 2594. [CrossRef]
30. Pathan, A.I.; Agnihotri, P.G. Application of new HEC-RAS version 5 for 1D hydrodynamic flood modeling with special reference through geospatial techniques: A case of River Purna at Navsari, Gujarat, India. *Model. Earth Syst. Environ.* **2021**, *7*, 1133–1144. [CrossRef]
31. Merwade, V.; Cook, A.; Coonrod, J. Gis techniques for creating river terrain models for hydrodynamic modeling and flood inundation mapping. *Environ. Model. Softw.* **2008**, *23*, 1300–1311. [CrossRef]

32. Sebastian, A.; Juan, A.; Bedient, P.B. Urban flood modeling: Perspectives, challenges, and opportunities. *Coast. Flood Risk Reduct.* **2022**, 47–60. [CrossRef]
33. Luo, P.; Luo, M.; Li, F.; Qi, X.; Huo, A.; Wang, Z.; He, B.; Takara, K.; Nover, D.; Wang, Y. Urban flood numerical simulation: Research, methods and future perspectives. *Environ. Model. Softw.* **2022**, *156*, 105478. [CrossRef]
34. Papaioannou, G.; Loukas, A.; Vasiliades, L.; Aronica, G.T. Flood inundation mapping sensitivity to riverine spatial resolution and modelling approach. *Nat. Hazards* **2016**, *83*, 117–132. [CrossRef]
35. Varra, G.; Della Morte, R.; Tartaglia, M.; Fiduccia, A.; Zammuto, A.; Agostino, I.; Booth, C.A.; Quinn, N.; Lamond, J.E.; Cozzolino, L. Flood susceptibility assessment for improving the resilience capacity of railway infrastructure networks. *Water* **2024**, *16*, 2592. [CrossRef]
36. Thaivalappil Sukumaran, S.; Birkinshaw, S.J. Investigating the impact of recent and future urbanization on flooding in an Indian River catchment. *Sustainability* **2024**, *16*, 5652. [CrossRef]
37. Trif, S.; Bilașco, Ș.; Petrea, D.; Roșca, S.; Fodorean, I.; Vescan, I. Spatial modeling through gis analysis of flood risk and related financial vulnerability: Case study: Turcu River, Romania. *Appl. Sci.* **2023**, *13*, 9869. [CrossRef]
38. Iroume, J.Y.-A.; Onguéné, R.; Djanna Koffi, F.; Colmet-Daage, A.; Stieglitz, T.; Essoh Sone, W.; Bogning, S.; Olinga Olinga, J.M.; Ntchantcho, R.; Ntonga, J.-C.; et al. The 21st August 2020 flood in Douala (Cameroon): A major urban flood investigated with 2D HEC-RAS modeling. *Water* **2022**, *14*, 1768. [CrossRef]
39. Arseni, M.; Rosu, A.; Calmuc, M.; Calmuc, V.A.; Iticescu, C.; Georgescu, L.P. Development of flood risk and hazard maps for the lower course of the Siret River, Romania. *Sustainability* **2020**, *12*, 6588. [CrossRef]
40. Al-Hussein, A.A.M.; Khan, S.; Ncibi, K.; Hamdi, N.; Hamed, Y. Flood analysis using HEC-RAS and HEC-HMS: A case study of Khazir River (Middle East-Northern Iraq). *Water* **2022**, *14*, 3779. [CrossRef]
41. Rojas, O.; Mardones, M.; Rojas, C.; Martínez, C.; Flores, L. Urban growth and flood disasters in the coastal river basin of South-Central Chile (1943–2011). *Sustainability* **2017**, *9*, 195. [CrossRef]
42. HEC-RAS User's Manual. Available online: https://www.hec.usace.army.mil (accessed on 12 October 2024).
43. Rangari, V.A.; Umamahesh, N.V.; Bhatt, C.M. Assessment of inundation risk in urban floods using HEC RAS 2D. *Model. Earth Syst. Environ.* **2019**, *5*, 1839–1851. [CrossRef]
44. Ongdas, N.; Akiyanova, F.; Karakulov, Y.; Muratbayeva, A.; Zinabdin, N. Application of HEC-RAS (2D) for flood hazard maps generation for Yesil (Ishim) river in Kazakhstan. *Water* **2020**, *12*, 2672. [CrossRef]
45. Namara, W.G.; Damisse, T.A.; Tufa, F.G. Application of HEC-RAS and HEC-GeoRAS model for flood inundation mapping, the case of Awash Bello flood plain, upper Awash River Basin, Oromiya regional state, Ethiopia. *Model. Earth Syst. Environ.* **2022**, *8*, 1449–1460. [CrossRef]
46. Peker, İ.B.; Gülbaz, S.; Demir, V.; Orhan, O.; Beden, N. Integration of HEC-RAS and HEC-HMS with gis in flood modeling and flood hazard mapping. *Sustainability* **2024**, *16*, 1226. [CrossRef]
47. Afzal, M.A.; Ali, S.; Nazeer, A.; Khan, M.I.; Waqas, M.M.; Aslam, R.A.; Cheema, M.J.M.; Nadeem, M.; Saddique, N.; Muzammil, M.; et al. Flood inundation modeling by integrating HEC–RAS and satellite imagery: A case study of the Indus River Basin. *Water* **2022**, *14*, 2984. [CrossRef]
48. Huţanu, E.; Mihu-Pintilie, A.; Urzica, A.; Paveluc, L.E.; Stoleriu, C.C.; Grozavu, A. Using 1D HEC-RAS modeling and lidar data to improve flood hazard maps accuracy: A case study from Jijia floodplain (NE Romania). *Water* **2020**, *12*, 1624. [CrossRef]
49. Bush, S.T.; Dresback, K.M.; Szpilka, C.M.; Kolar, R.L. Use of 1D unsteady HEC-RAS in a coupled system for compound flood modeling: North Carolina case study. *J. Mar. Sci. Eng.* **2022**, *10*, 306. [CrossRef]
50. Tayefi, V.; Lane, S.N.; Hardy, R.J.; Yu, D. A comparison of one-and two-dimensional approaches to modelling flood inundation over complex upland floodplains. *Hydrol. Process. Int. J.* **2007**, *21*, 3190–3202. [CrossRef]
51. Yazdan, M.M.S.; Ahad, M.T.; Kumar, R.; Mehedi, M.A.A. Estimating flooding at river spree floodplain using HEC-RAS simulation. *J.* **2022**, *5*, 410–426. [CrossRef]
52. Patel, D.P.; Ramirez, J.A.; Srivastava, P.K.; Bray, M.; Han, D. Assessment of flood inundation mapping of Surat city by coupled 1D/2D hydrodynamic modeling: A case application of the new HEC-RAS 5. *Nat. Hazards* **2017**, *89*, 93–130. [CrossRef]
53. Bruno, L.S.; Mattos, T.S.; Oliveira, P.T.S.; Almagro, A.; Rodrigues, D.B.B. Hydrological and hydraulic modeling applied to flash flood events in a small urban stream. *Hydrology* **2022**, *9*, 223. [CrossRef]
54. Vozinaki, A.E.K.; Morianou, G.G.; Alexakis, D.D.; Tsanis, I.K. Comparing 1D and combined 1D/2D hydraulic simulations using high-resolution topographic data: A case study of the Koiliaris basin, Greece. *Hydrolog. Sci. J.* **2017**, *62*, 642–656. [CrossRef]
55. DSI. Hydrometric Measurement Guidelines. Ministry of Agriculture and Forestry, General Directorate of State Hydraulic Works. Available online: https://cdniys.tarimorman.gov.tr/api/File/GetGaleriFile/425/DosyaGaleri/1456/hidrometrikolcumyonergesi.pdf (accessed on 3 September 2024).
56. MFWA. Ministry of Forestry and Water Affairs, General Directorate of Water Management, Antalya Basin Flood Management Plan. Available online: https://www.tarimorman.gov.tr/ (accessed on 12 October 2024).

57. Erdoğan, B.U.; Salış, O.B. Spatio-temporal analysis of land use and land cover changes in boğaçayi watershed in a touristic region in Turkey. *Environ. Eng. Manag. J.* **2023**, *22*, 183–197. [CrossRef]
58. Climate Data. Climate of Konyaalti. Available online: https://tr.climate-data.org/ (accessed on 11 October 2024).
59. Kahraman, E. Effect of Constructed Wetlands on Urban Ecosystem: The Case of Antalya-Konyaaltı. PhD Thesis, Burdur Mehmet Akif Ersoy University, Burdur, Turkey, 2023.
60. Official Climate Statistics. Available online: https://www.mgm.gov.tr/veridegerlendirme/il-ve-ilceler-istatistik.aspx?m=ANTALYA (accessed on 22 October 2024).
61. Google Earth. Available online: https://earth.google.com/web/ (accessed on 17 October 2024).
62. Antalya Governorship. Provincial Disaster and Emergency Directorate, Provincial Disaster Risk Reduction Plan. Available online: https://antalya.afad.gov.tr/kurumlar/antalya.afad/Tasarim/IRAP/Antalya-IRAP_2022.pdf (accessed on 16 September 2024).
63. ASF. Alaska Satellite Facility. Available online: https://asf.alaska.edu/ (accessed on 9 September 2024).
64. HEC-RAS. US Army Corps of Engineers, Hydrologic Engineering Center. Available online: https://www.hec.usace.army.mil/software/hec-ras/download.aspx (accessed on 23 September 2024).
65. Sanz-Ramos, M.; Bladé, E.; González-Escalona, F.; Olivares, G.; Aragón-Hernández, J.L. Interpreting the manning roughness coefficient in overland flow simulations with coupled hydrological-hydraulic distributed models. *Water* **2021**, *13*, 3433. [CrossRef]
66. Garrote, J.; González-Jiménez, M.; Guardiola-Albert, C.; Díez-Herrero, A. The manning's roughness coefficient calibration method to improve flood hazard analysis in the absence of river bathymetric data: Application to the urban historical Zamora City Centre in Spain. *Appl. Sci.* **2021**, *11*, 9267. [CrossRef]
67. Cowan, W.L. Estimating hydraulic roughness coefficients. *Agric. Eng.* **1956**, *37*, 473–475.
68. Demir, V.; Keskin, A.Ü. Determination of manning roughness coefficient by cowan method and remote sensing. *Gazi J. Eng. Sci.* **2019**, *5*, 167–177. [CrossRef]
69. ESRI. ArcGIS Living Atlas of the World. Available online: https://livingatlas.arcgis.com/en/home/ (accessed on 10 October 2024).
70. Karra, K.; Kontgis, C.; Statman-Weil, Z.; Mazzariello, J.C.; Mathis, M.; Brumby, S.P. Global Land Use/Land Cover With Sentinel 2 and Deep Learning. In Proceedings of the 2021 IEEE International Geoscience and Remote Sensing Symposium IGARSS, Brussels, Belgium, 11–16 July 2021; pp. 4704–4707.
71. Du, S.; Xiong, Z.; Wang, Y.C.; Guo, L. Quantifying the multilevel effects of landscape composition and configuration on land surface temperature. *Remote Sens. Environ.* **2016**, *178*, 84–92. [CrossRef]
72. Tveit, M.; Ode, Å.; Fry, G. Key concepts in a framework for analysing visual landscape character. *Landsc. Res.* **2006**, *31*, 229–255. [CrossRef]
73. Chen, J.; Gao, C.; Zhou, H.; Wang, Q.; She, L.; Qing, D.; Cao, C. Urban flood risk assessment based on a combination of subjective and objective multi-weight methods. *Appl. Sci.* **2024**, *14*, 3694. [CrossRef]
74. Kundzewicz, Z.W.; Kanae, S.; Takeuchi, K. Flood risk and climate change: The need for an integrated approach. *Hydrol. Sci. J.* **2019**, *64*, 607–617.
75. Peters, D.P.C.; Okin, G.S.; Whitford, W.G. Impacts of flooding on soil and vegetation dynamics in arid environments. *Ecol. Appl.* **2017**, *27*, 1647–1660.
76. Smith, J.R.; Johnson, P. Vegetation response to flooding: Implications for ecosystem management. *Ecol. Manag. Aquat. Veg.* **2020**, *1*, 15–28.
77. Miller, M. The effects of flooding on aquatic and terrestrial ecosystems: A review. *Wetl. Ecol. Manag.* **2018**, *26*, 257–267.
78. Olson, K.R. Impacts of 2008 flooding on agricultural lands in Illinois, Missouri, and Indiana. *J. Soil Water Conserv.* **2009**, *64*, 167–171. [CrossRef]
79. Gupta, S.K.; Bantawa, P.; Rai, S.; Ali, S.; Pradhan, J.; Lama, S.B.; Rai, R. Enhancing citrus resilience: Strategies and advances in abiotic stress management: A review. *Indian J. Agric. Res.* **2024**, *58*, 953. [CrossRef]
80. Rodríguez-Gamir, J.; Ancillo, G.; González-Mas, M.C.; Primo-Millo, E.; Iglesias, D.J.; Forner-Giner, M.A. Root signalling and modulation of stomatal closure in flooded citrus seedlings. *Plant Physiol. Biochem.* **2011**, *49*, 636–645. [CrossRef] [PubMed]
81. Graham, J.; Feichtenberger, E. Citrus phytophthora diseases: Management challenges and successes. *J. Citrus Pathol.* **2015**, *2*, 1–11. [CrossRef]
82. Aygören, E. Product Report Citrus 2023. Available online: https://arastirma.tarimorman.gov.tr/ (accessed on 12 October 2024).
83. Haq, M.U.; Koc, M.; Ture, M. Green infrastructure as a sustainable approach for flood management: A case study. *Landsc. Urban Plan.* **2021**, *204*, 103918.
84. Selim, S.; Dönmez, B.; Kilçik, A. Determination of the optimum number of sample points to classify land cover types and estimate the contribution of trees on ecosystem services using the I-Tree Canopy tool. *Integr. Environ. Assess. Manag.* **2023**, *19*, 726–734. [CrossRef]
85. Xu, K.; Fang, J.; Fang, Y.; Sun, Q.; Wu, C.; Liu, M. The importance of digital elevation model selection in flood simulation and a proposed method to reduce DEM errors: A case study in Shanghai. *Int. J. Disaster Risk Sci.* **2021**, *12*, 890–902. [CrossRef]

86. Try, S.; Tanaka, S.; Tanaka, K.; Sayama, T.; Khujanazarov, T.; Oeurng, C. Comparison of CMIP5 and CMIP6 GCM performance for flood projections in the Mekong River Basin. *J. Hydrol. Reg. Stud.* **2022**, *40*, 101035. [CrossRef]
87. Shen, Y.; Jiang, C. A comprehensive review of watershed flood simulation model. *Nat. Hazards* **2023**, *118*, 875–902. [CrossRef]
88. Mahmoodi, E.; Azari, M.; Dastorani, M.T.; Salvati, A. Comparison of hydrological modeling, artificial neural networks and multi-criteria decision making approaches for determining flood source areas. *Water Resour. Manag.* **2024**, *38*, 5343–5363. [CrossRef]
89. Kabir, S.; Patidar, S.; Xia, X.; Liang, Q.; Neal, J.; Pender, G. A deep convolutional neural network model for rapid prediction of fluvial flood inundation. *J. Hydrol.* **2020**, *590*, 125481. [CrossRef]
90. Zhou, Y.; Wu, W.; Nathan, R.; Wang, Q.J. A rapid flood inundation modelling framework using deep learning with spatial reduction and reconstruction. *Environ. Model. Softw.* **2021**, *143*, 105112. [CrossRef]
91. Donnelly, J.; Abolfathi, S.; Pearson, J.; Chatrabgoun, O.; Daneshkhah, A. Gaussian process emulation of spatio-temporal outputs of a 2D inland flood model. *Water Res.* **2022**, *225*, 119100. [CrossRef]
92. Hu, R.; Fang, F.; Pain, C.C.; Navon, I.M. Rapid spatio-temporal flood prediction and uncertainty quantification using a deep learning method. *J. Hydrol.* **2019**, *575*, 911–920. [CrossRef]
93. Aryal, A.; Acharya, A.; Kalra, A. Assessing the implication of climate change to forecast future flood using CMIP6 climate projections and HEC-RAS modeling. *Forecasting* **2022**, *4*, 582–603. [CrossRef]
94. Zainal, N.N.; Talib, S.H.A. Review paper on applications of the HEC-RAS model for flooding, agriculture, and water quality simulation. *Water Pract. Technol.* **2024**, *19*, 2883–2900. [CrossRef]

Disclaimer/Publisher's Note: The statements, opinions and data contained in all publications are solely those of the individual author(s) and contributor(s) and not of MDPI and/or the editor(s). MDPI and/or the editor(s) disclaim responsibility for any injury to people or property resulting from any ideas, methods, instructions or products referred to in the content.